J Nanopart Res (2025) 27:188
https://doi.org/10.1007/s11051-025-06379-y

RESEARCH

Magnetite nanoparticles doped with rare earth ions: synthesis, structural, and magnetic properties

A. V. Rutkauskas · O. N. Lis · S. E. Kichanov · E. V. Lukin · B. A. Abdurakhimov · G. S. Rymski · A. L. Zhaludkevich · I. I. Makoed · D. P. Kozlenko · A. Mutali

Received: 31 March 2025 / Accepted: 15 June 2025

Abstract Taking into account the practical significance of magnetite nanoparticles, several nanostructured magnetite samples with doping of 2.5% Sm, Dy, La, and Lu rare earth ions were synthesized using the co-precipitation method. The structural and magnetic properties of the obtained doped nanoparticles were investigated in detail using transmission electron microscopy, X-ray diffraction, small-angle X-ray scattering, and magnetic measurements. All the doped nanostructured magnetite samples have a cubic phase with spinel crystal structure $Fd\ \bar{3}\ m$; a nanoparticle size is ranging from 20 to 32 nm. Changes in the characteristic Fe–O bond lengths indicated that the doping rare earth ions mainly occupy octahedral sites in the oxygen unit. The size of the nanoparticles depends on the type of doped rare earth due to difference in ionic radius. Neutron diffraction data indicated that the magnetic structure of doped magnetite nanoparticles is ferrimagnetic. The magnetic measurements showed a superparamagnetic state in all the doped magnetite nanoparticles. It is assumed that noticeable changes in the structural and magnetic properties of magnetite nanoparticles compared to bulk matter are primarily associated with a defect-rich structure on the surface of those nanoparticles and the effect of rare earth ions doping on it.

Keywords Magnetite nanoparticles · Rare earth ions · Magnetic resonance imaging

A. V. Rutkauskas (✉) · O. N. Lis · S. E. Kichanov · E. V. Lukin · B. A. Abdurakhimov · D. P. Kozlenko
Frank Laboratory of Neutron Physics, Joint Institute for Nuclear Research, 141980 Dubna, Russia
e-mail: ranton@nf.jinr.ru

O. N. Lis
Institute of Physics, Kazan Federal University, 420008 Kazan, Russia

G. S. Rymski · A. L. Zhaludkevich
Scientific-Practical Materials Research Centre of the National Academy of Sciences of Belarus, 220072 Minsk, Belarus

I. I. Makoed
Brest State A.S. Pushkin University, 224016 Brest, Belarus

A. Mutali
Flerov Laboratory of Nuclear Reactions, Joint Institute for Nuclear Research, 141980 Dubna, Russia

Introduction

Magnetite Fe_3O_4 is the oldest known magnetic mineral and has played a significant role in both natural processes and technological advances [22],de Jesus Andrade Fidelis et al. [9]). The evolution of its applications has a long historical path from ancient compasses used for navigation three thousand years ago to modern developments in nanotechnology such as spin valves, magnetoresistive memory [11], medical diagnostics and treatment [43, 59, 66], as well as contrast agents [20] for enhancing data in magnetic resonance imaging [8]. Due to its outstanding

Published online: 04 July 2025

magnetic properties, biocompatible magnetite nanoparticles have great potential for use in hyperthermia therapy [53, 66, 68], where an external magnetic field causes cancer cells to become so hot that they are destroyed while the surrounding healthy tissues remain unaffected.

In recent years, various methods have been proposed for controlling the properties of magnetite nanoparticles [41]. These methods include the nanoparticle synthesis approach and the chemical doping of magnetite with rare earth (RE) elements [48],de Jesús Ibarra–Sánchez et al. [10]; [31, 69]. The substitution by a RE ion in a magnetite nanoparticle significantly affects their physical properties and improves their magnetic characteristics. And first of all, it is related to a decrease in the concentration of Fe^{3+} ions in octahedral or tetrahedral crystallographic sites in the spinel crystal lattice and a partial suppression of the interaction between the iron magnetic moments (Li et al. [48]). It should be noted that the orbital contributions to the magnetic moment are more significant for RE ions, due to smaller crystal-field effects and stronger spin-orbital coupling for the *f*-electrons of rare earth ions compared to the *d*-electrons for transition metals (Li et al. [21]). From a structural standpoint, the addition of RE elements to the cubic spinel structure of magnetite modifies the Fe–Fe interactions and creates new magnetic interactions between RE and Fe. This leads to changes in the saturation magnetization of nanostructured magnetite materials [26, 28, 51, 52]. In addition, the *4f* orbitals of RE elements are vacant and can be filled with electrons, providing additional opportunities for novel phenomena in magnetism (Li et al. [40]) and optical properties. It is assumed that the degree of impact on the magnetic properties of magnetite nanoparticles is related not only to the distribution of rare earth ions in the spinel-type crystal structure but also to the type of dopant element [58]. For example, substitution of Fe^{3+} ions with La^{3+} ions with a larger ion radius leads to a more significant reduction in saturation magnetization than for the smaller dysprosium Dy^{3+} ions [31]. Doping with rare earth elements leads to changes in the optical properties of magnetite nanoparticles. Thus, the doping process causes absorption peak shifting and an increase in the optical band gap. Therefore, the doped magnetite nanoparticles become more suitable for use in photocatalytic applications [30].

On the other hand, the magnetic properties of magnetite nanoparticles are affected by nanostructural features, such as particle size, shape, or surface-related characteristics [41, 65, 67]. When the size of magnetic nanoparticles decreases below ~ 60 nm, magnetite nanoparticles become single-domain magnetic particles [41, 65]. With particle sizes less than 40–50 nm, magnetite nanostructured materials are in a superparamagnetic state at room temperature [65], which is associated with coherent spin reversal of individual nanoparticle moments [16]. The magnetite nanoparticles doped with rare-earth ions exhibit advanced properties due to enhanced magnetic relaxation caused by the presence of additional structural disorder on the particle surface [35]. This structural disorder corresponds to surface defects that can give rise to local spin-glass magnetic states [35].

Taking into account the practical use of magnetite nanoparticles doped with rare earth elements, research teams are actively developing new methods or optimizing already known techniques for the synthesis of these magnetic nanoparticles. And here, it should be noted that doped magnetite nanoparticles can aggregate due to strong interparticle interaction caused by magnetic forces [6, 55]. Efforts to improve the synthesis of magnetite nanoparticle are aimed at precisely preventing agglomeration of individual particles, which can cause uniformity in the size distribution of nanoparticles and a decline in the magnetic properties of nanostructured system. In the sol–gel approach [3], nanoparticle size is controlled by selecting precursors, chousing hydrolysis and gelation conditions, and adding surfactants or polymers to stabilize the particles and prevent agglomeration. Microemulsions [15] are a type of system that is thermodynamically stable and consists of two liquids that do not mix, with one liquid being dispersed as droplets in the other. By adjusting the composition and conditions of microemulsions, the size of nanoparticles can be controlled. In laser ablation method [57], a laser beam is employed to vaporize material from a surface, and by adjusting the energy and duration of the beam, we regulate the resulting nanoparticles size. Chemical vapor deposition method [39] allow us to control particle size by changing pressure, temperature, gas composition, or gas flow rate. Electrochemical synthesis [18] provide opportunities to control particle size through the choice of electrodes, current

density, electrolyte composition, and other process parameters.

Despite a wide range of methods for the synthesizing of nanoparticles of doped magnetite, all of these approaches must meet the criteria for economic viability [60]. This means that the synthesizing of doped magnetite nanoparticles can be relatively inexpensive, requiring cheap reagents, equipment, and reproducible chemical processes. From this perspective, the classical co-precipitation method [4] is attractive. This technique allows controlling particle size by adjusting parameters such as reaction temperature, pH of the medium, concentration of reagents, and mixing rate. Changing these parameters allows control over the size of formed nanoparticles. We synthesized several sets of magnetite nanoparticles with different types of introduced RE ions: Sm^{3+}, Lu^{3+}, La^{3+}, and Dy^{3+}, under the same co-precipitation synthesis conditions and at the same concentration of rare earth elements. The structural and magnetic properties of the doped magnetite nanoparticles were investigated using transmission electron microscopy, X-ray small-angle scattering, X-ray and neutron diffraction, and magnetic susceptibility measurements.

Experimental

Nanoparticles of undoped magnetite Fe_3O_4 and magnetite with Sm^{3+}, Lu^{3+}, La^{3+}, and Dy^{3+} ions were synthesized using the co-precipitation method. For the synthesis of magnetite, the iron Fe(III) chloride hexahydrate ($FeCl_3{\cdot}6H_2O$) and Fe(II) sulfate heptahydrate ($FeSO_4{\cdot}7H_2O$) were used as starting materials, which were mixed in stoichiometric ratios (Fe^{3+}: Fe^{2+} =2:1 mol). Rare earth nitrate tetrahydrate ($RE(NO_3)_3{\cdot}4H_2O$) was used to prepare the substituted compounds. Aqueous solutions were mixed in a molar ratio of 1.925:1.00:0.075 for 2.5 at.% of doped rare earth content. The reaction was carried out in an N_2 atmosphere to avoid partial oxidation of Fe^{2+} to α-FeOOH. The 25% solution of ammonia NH_4OH was used as a precipitating agent. As a result of synthesis, the black matter particles were obtained. A testing X-ray diffraction analysis provides a single phase with cubic spinel structure of $Fd\,\bar{3}\,m$ space group, which was confirmed by further diffraction experiments. For our research, we selected four doped magnetite compounds Fe_3O_4:Sm, Fe_3O_4:Lu, Fe_3O_4:La and Fe_3O_4:Dy with the same concentration of rare earth ion of 2.5 at.%.

For TEM sample preparation, the powder was dispersed in 10 mL of ethanol, sonicated in a Bandelin ultrasonic bath for 10 min, and further processed for 15 min using an I10-840 disperser (22 kHz, 30% amplitude, 10-s pulses with 2-s pauses). To optimize nanoparticle concentration, the suspension was centrifuged at 500 g for 5 min using an MPW-352 centrifuge. Subsequently, 15 μL of the suspension was deposited onto carbon-coated TEM grids. The morphology and size of the obtained magnetite nanoparticles were studied using the transmission electron microscope (TEM) using a FEI Talos™ F200i S/TEM (Waltham, MA, USA) operated at 200 kV at the FLNR, JINR (Dubna, Russia).

Small-angle X-ray scattering (SAXS) is a valuable method for characterizing the structural features of nanoparticles [42]. X-ray small-angle scattering and X-ray diffraction experiments were performed using the Xeuss 3.0 instrument (located in the FLNP, JINR, Russia) manufactured by XENOCS (Grenoble, France). The radiation was emitted from the GeniX3D source (Mo-Kα edge, λ=0.71078 Å). Small-angle X-ray scattering spectra were acquired using an Eiger2 detector at various distances between the sample and detector, ranging from 1.0 to 4.0 m. The SAXS spectra were corrected for the data obtained from the empty container. The analysis of the small-angle scattering data was performed using the SasView [2] and McSAS [50] software.

Neutron diffraction experiments were prepared using the DN-12 diffractometer [34] at the IBR-2 pulsed reactor (FLNP, JINR, Russia). Typical experimental time for each sample was 4 h. The X-ray and neutron diffraction experimental data were refined using Fullprof software [54].

A measurement of magnetic field dependences of magnetization was studied using the Cryogenic vibration magnetometer (Cryogenic Limited, UK) in the temperature range from 4 to 300 K, in a magnetic field up to 3 T.

Results

Transmission electron microscopy

The obtained TEM images of the studied nanostructured compounds are presented in Fig. 1. It can be

seen that all the nanoparticles are round-shaped grains with an average size of approximately 20–30 nm. Even well-defined spherical nanoparticles are characteristic for undoped nanostructured Fe_3O_4 magnetite, while larger particles with a rougher surface are observed for RE doped ones. The size of studied nanoparticles was simple estimated by analyzing TEM images using the software ImageJ [56]. The calculated size distribution histograms are presented in the inserts of Fig. 1.

The size distribution histogram was fitted using the normal distribution function. Generalized envelopes of the size distributions for the magnetite nanoparticles are shown in Fig. 2. The average

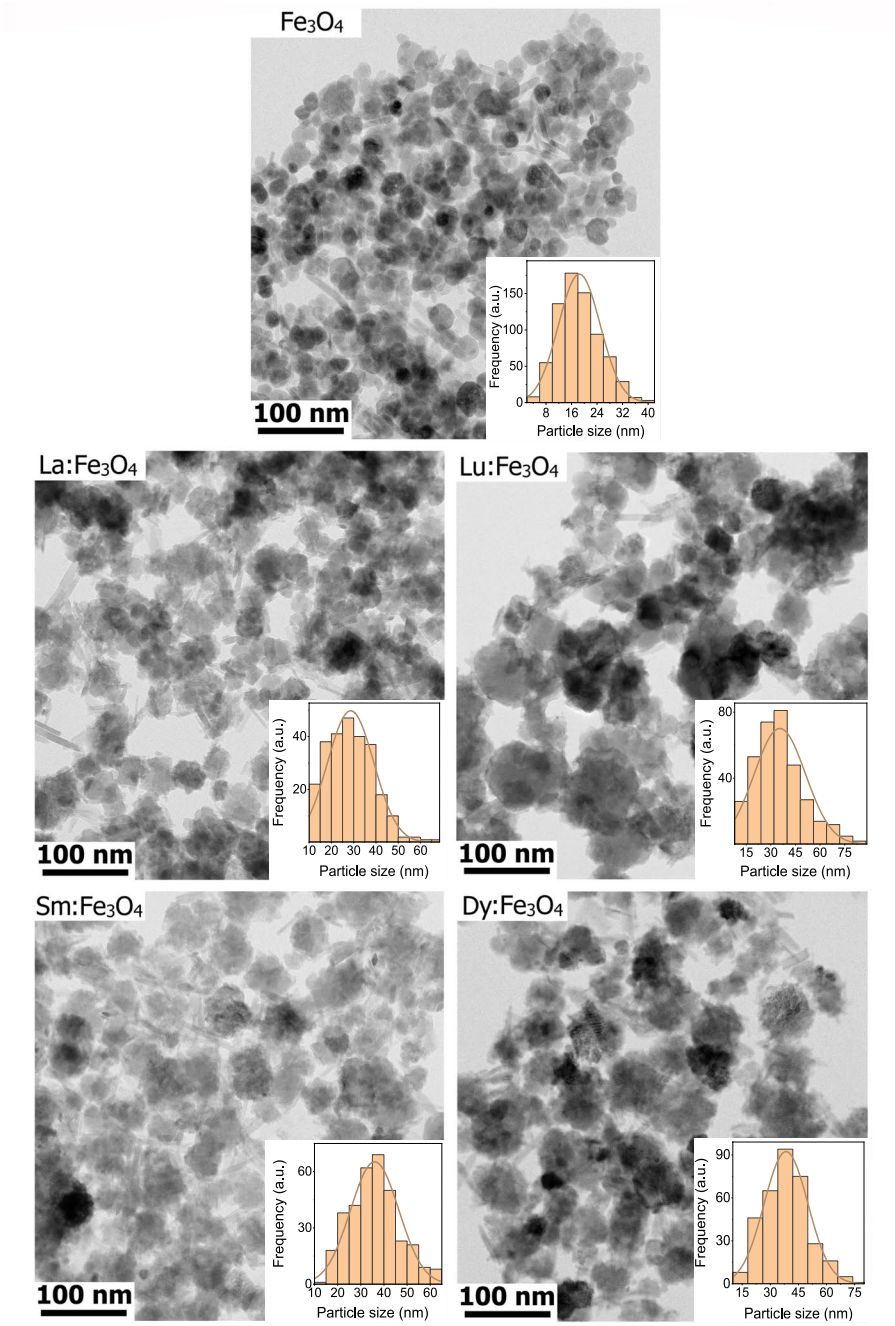

Fig. 1 Transmission electron microscope images with the size distribution histogram of doped magnetite nanoparticles of Fe_3O_4, La:Fe_3O_4, Lu:Fe_3O_4, Sm:Fe_3O_4, and Dy:Fe_3O_4

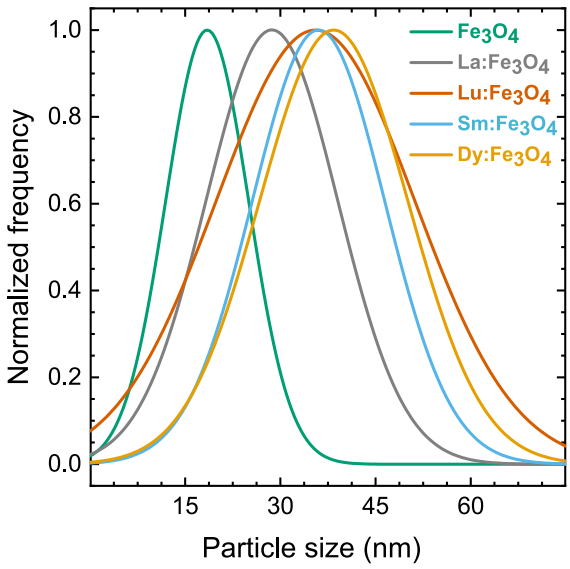

Fig. 2 The obtained normalized average particles size distribution curves of doped magnetite nanoparticles

diameter of undoped Fe_3O_4 nanoparticles is estimated as 19 ± 3 nm. Doped magnetite nanoparticle sizes are larger, with an average size 28 ± 5 nm for La:Fe_3O_4; 35 ± 5 nm for Lu:Fe_3O_4; 35 ± 5 nm for Sm:Fe_3O_4; 38 ± 12 nm for Dy:Fe_3O_4. Aggregates formed from individual nanoparticles show solder bonds between them, resulting in an increase in the average particle size.

Small-angle X-ray scattering

For a more in-depth analysis of the average size and size distribution of doped magnetite nanoparticles, a small-angle X-ray scattering technique was employed. The SAXS spectra obtained for the nanostructured doped magnetites are shown in Fig. 3. The SAXS data presents the scattered intensity as a function of the momentum transfer q, which is defined as $(4\pi/\lambda)\sin\theta$, where θ is the scattering angle and λ is the wavelength of incident X-rays [62]. The obtained SAXS curves for magnetite nanoparticle samples are similar and have a typical shape, which is characteristic of scattering from typical fractal systems [63]. There are slight variations in the degree of slope of the SAXS curves and their shape, which may correspond to changes in fractal dimensions of scattering objects. And as a first approximation, to obtain the average size of magnetite nanoparticles, we fit the SAXS data using the equation of the unified exponential-power law model of Beaucage [5, 19]:where the fitting coefficients G and B, the radius of gyration R_g, and the exponents of the power-law decrease P are fitting parameters in the scattering law $I(q)$ for the magnetite nanoparticles. The variable Q^* is renormalized in the power law [5, 19]:

$$I(q) = \text{background} + G\exp\left(\frac{-q^2R_g^2}{3}\right) + B\exp\left(\frac{-q^2R_g^2}{3}\right)\left(\frac{1}{Q^*}\right)^P, \quad (1)$$

Equation (1) was used to estimate the radius of gtration R_g of the magnetite nanoparticles, which is the average radius r of a nanoparticle in a spherical approximation as $R_g = \sqrt{\frac{3}{5}}r$ [62].

$$Q_1^* = \frac{q}{\left[\text{erf}\left(\frac{qR_g}{\sqrt{6}}\right)\right]^3}. \quad (2)$$

The obtained radii of gyration and the sphere-model radii of doped nanoparticles are listed in Table 1. The size values are close to those obtained earlier for nanoparticles synthesized using the hydrothermal method (Paula [49]). Also, the calculated values for the power-law exponents P in Eq. (1) are presented in Table 1. These parameters relate to the fractal dimension of the nanostructured system. The exponent P varies slightly between 3.4 and 3.8, which indicates surface fractals with smooth and sharp interface. These conclusions are confirmed by TEM data presented above.

It can be seen that the average size of nanoparticles, according to the SAXS data (Table 1), is slightly larger than that the cristallite sizes obtained from the analysis of X-ray diffraction data ("X-ray diffraction" 3.3). This may be due to the aggregation of nanoparticles.

To further analyze the dimensional distribution of nanoparticles, we used the capabilities of the Martelli Monte Carlo method [13] for SAXS data processing. These methods based on random updates are suitable for retrieving form-free nanoparticle size distributions [50]. The resulting size

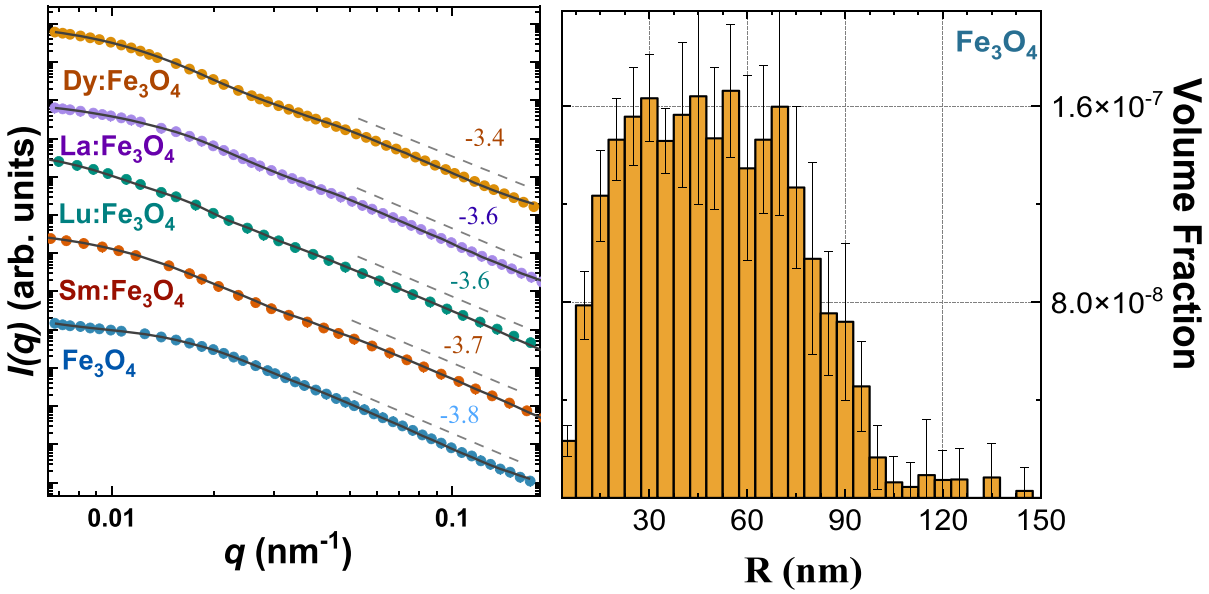

Fig. 3 **a** The obtained SAXS curves of doped magnetite nanoparticles. The experimental points and fitting profiles based on Eq. (2) calculations are presented. The dotted line indicates the slope of the SAXS curve. **b** The size distributions for the undoped magnetite nanoparticles obtained from SAXS data analysis using the McSAS [50] software

distributions of the studied doped magnetite nanoparticles are shown in the Fig. 4. It can be seen that all the studied compounds have a fairly wide range of sizes, up to several tens of nanometers. However, when we look at the undoped magnetite data, we see a distribution that is closer to a Gaussian shape. For nanoparticles doped with rare earth elements, a bimodal distribution is more typical (Fig. 4). At the same time, there is a shape peak in the range of small sizes, and for all doped nanoparticles, a wide peak is observed for aggregates up to 100 nm in size. The bimodal size distribution can indicate the formation of aggregates of the magnetite nanoparticles. It can be assumed that, when rare earth elements are embedded into magnetite nanoparticles, the surface of the nanoparticles is modified [31, 38]. This serves as an additional factor for chemical bonding between nanoparticles. In addition, magnetic interactions between nanoparticles takes place.

Table 1 The calculated size parameters for doped magnetite nanoparticles obtained by fitting the SAXS data using the function (2)

Sample	R_g, *nm*	*r, nm*	*P*
Fe_3O_4	11.99(26)	15.47(26)	3.82(2)
Fe_3O_4:*La*	15.88(34)	20.50(34)	3.59(4)
Fe_3O_4:*Lu*	18.46(23)	18.46(23)	3.68(4)
Fe_3O_4:*Sm*	18.29(33)	18.29(33)	3.70(3)
Fe_3O_4:*Dy*	19.47(20)	19.47(20)	3.41(3)

X-ray diffraction

The X-ray diffraction patterns of nanostructured magnetite are shown in Fig. 5a. All studied nanostructured samples are characterized by similar diffraction patterns. The analysis of the data showed that the diffraction peaks of the samples can be completely indexed in a cubic spinel structure with the $Fd\,\bar{3}\,m$ space group [14, 29]. No unindexed reflections were found in any of the XRD patterns for all studied compounds, indicating that the samples are single-phase with no noticeable secondary phases.

The lattice parameters of the cubic structure of doped magnetite were calculated from the XRD data (Table 2). With an increase in the ionic radius of the dopant from 0.55 Å for Fe^{3+} to 1.061 Å for La^{3+}, a decrease in the lattice parameter is observed (Table 2), which may be attributed to the presence of a disordered and defect-rich structure on the

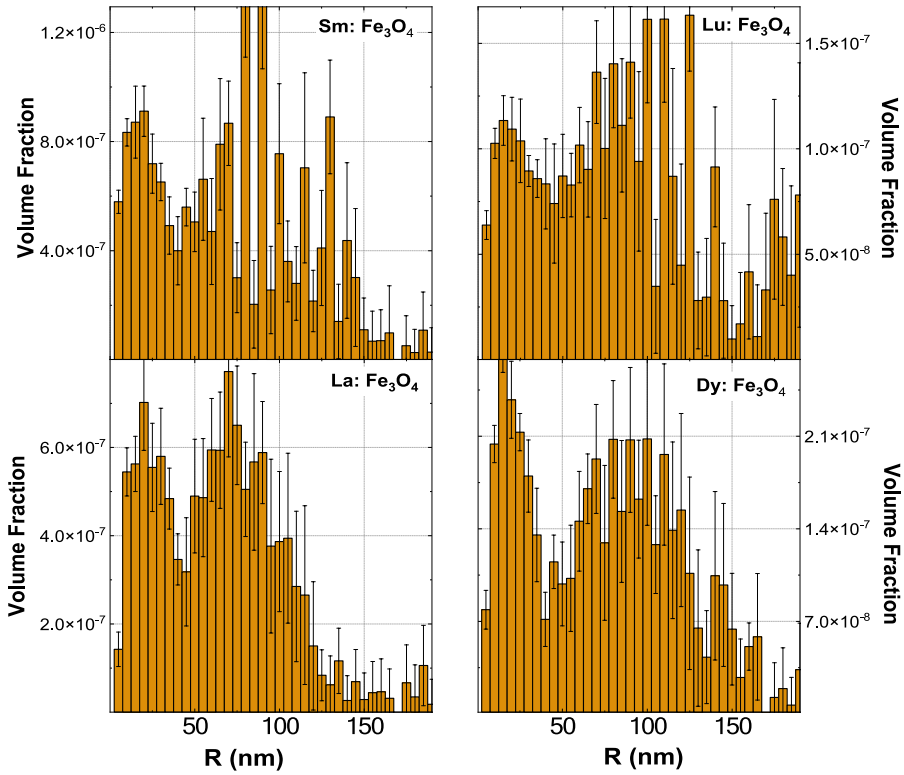

Fig. 4 The size distributions for the studied doped magnetite nanoparticles obtained from SAXS data

nanoparticle surfaces [12, 36]. Furthermore, this defect-rich structure leads to an increase in the average lattice parameter of the cubic magnetite structure. Surface defects, primarily composed of oxygen vacancies, lead to an increase in the lattice parameter of the spinel crystal structure, while the stabilization of these defects by RE dopants reduces the unit cell parameters, as previously reported [64].

Also, the average crystallite size of nanostructured magnetite was calculated using the modified Scherrer equation [45]. Taking the logarithm of both sides of the basic Scherrer formula, we can be express it as:

$$\ln\beta = \ln\frac{k\lambda}{L} + \ln\frac{1}{\cos\theta} \tag{3}$$

where L is the average crystallite size, k is the crystallite shape factor is usually taken as 0.9 [37], and λ is the X-ray wavelength ($\lambda = 0.071078$ nm), θ is the diffraction angle, as well as $\beta = \sqrt{\mathrm{FWHM}^2_{\mathrm{exp}} - \mathrm{FWHM}^2_{\mathrm{inst}}}$ is the full width at half maximum for the Gaussian

Table 2 The obtained lattice parameters, crystallite size, and lattice strains for nanostructured magnetite and doped RE:Fe_3O_4 (RE = La, Lu, Dy, Sm) nanoparticles. The X-ray and neutron diffraction data was analyzed within the cubic phase with space group Fd $\bar{3}$ m with the atomic positions of A-site 8a (1/8, 1/8, 1/8), B-site16d (½, ½, ½), and oxygen O 32e (x_O, x_O, x_O). The calculated magnetic moments were obtained from neutron diffraction data for doped magnetite nanoparticles

Sample	Lattice parameter (Å)	Crystallite size, L (nm)	Lattice strain, ε	x_O	$m_{A,}\ \mu_B$	$m_{B,}\ \mu_B$
Fe_3O_4	8.361(2)	14.7(2)	−0.0051(1)	0.2460(3)	1.11(2)	0.91(3)
La:Fe_3O_4	8.341(2)	19.8(3)	0.00259(1)	0.2455(4)	1.39(1)	1.00(3)
Lu:Fe_3O_4	8.351(1)	16.4(3)	0.00310(2)	0.2401(2)	1.34(3)	1.50(2)
Dy:Fe_3O_4	8.335 (2)	17.9(2)	0.00415(1)	0.2437(4)	1.30(2)	1.28(2)
Sm:Fe_3O_4	8.328(1)	15.3(3)	0.00772(1)	0.2477(5)	1.22(1)	0.92(3)

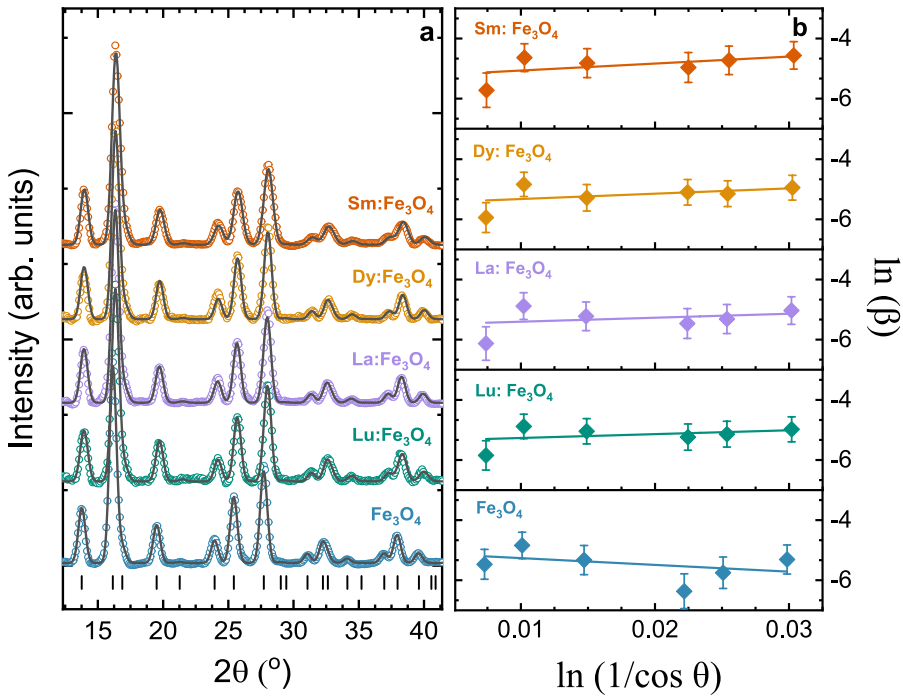

Fig. 5 **a** The X-ray diffraction patterns of undoped and doped RE:Fe_3O_4 (RE = La, Lu, Dy, Sm) nanostructured magnetites. The experimental data and calculated profiles using Rietveld method are shown. The ticks below represent the calculated positions of the diffraction peaks of the cubic phase Fd $\bar{3}$ m. **b** Linear plots of the modified Scherrer Eq. (3) for nanostructured magnetite

profile. The instrumental broadening $FWHM_{inst}$ contribution was determined experimentally from the diffraction spectrum of the fine-grained LaB_6 standard. To calculate the crystallite size, we plotted the dependence of $\ln\beta$ on $\ln(1/\cos\theta)$ and obtained the intercept after a linear fit of the points (Fig. 5b).

The obtained values of the average crystallite size are listed in Table 1. The doping of rare earth elements into the magnetite crystal lattice leads to a shrinking of the lattice and a slight increase in the crystallite size. It should be noted that the calculated sizes of crystallites are somewhat smaller than the sizes of nanoparticles (see the "Transmission electron microscopy" section). Moreover, this observation is consistent with the intrinsic characteristics of nanostructured particles, where the interior of the grains tends to be relatively free of defects, while defects are typically present at the grain surfaces [46].

Due to differences in the ion radii of iron and rare earth ions, local lattice distortions and strains can occur. It should be noted that lattice strains ε are inversely proportional to crystallite sizes in nanostructured ferrites [44]. Instead, the local distortions and lattice strains are determined to a greater extent by the distribution of rare earth RE and iron cations at the A and B sites in the spinel structure [24].

Neutron powder diffraction

Neutron diffraction patterns of nanostructured magnetites RE:Fe_3O_4 (RE = La, Lu, Dy, Sm), measured at ambient conditions, are shown in Fig. 6. In accordance with X-ray diffraction data, all the measured samples have the spinel-type crystal structure with $Fd\ \bar{3}\ m$ symmetry. The parameter x_O describes the centrality of the oxygen atom within its coordination sphere, and its typical value falls between 0.240 and 0.247 [47, 61]. The average value of $x_O \sim 0.24(2)$ does not practically change at RE doping (Table 2), which indicates the preservation of a normal spinel type with Fe^{2+} occupying the A site and Fe^{3+} occupying the B sites [17].

When doped with rare earth ions, we can expect significant influence on the magnetic exchange interactions within each of the A (J_{AA}) and B (J_{BB}) sublattices, as well as between the two sublattices J_{AB} in the magnetite crystal lattice [33]. From neutron diffraction data analysis, the values of iron

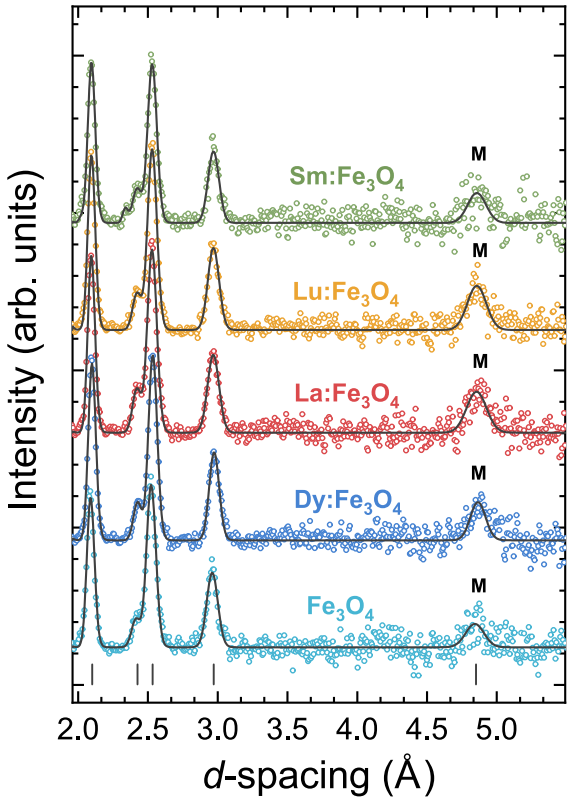

Fig. 6 The neutron diffraction patterns of magnetite nanoparticles doped with rare earth elements. The experimental points and calculated profiles by the Rietveld method are shown. The ticks mark the calculated positions of nuclear peaks for the cubic spinel crystal structure. The "M" signs the diffraction peak (111) with strongest magnetic contribution

magnetic moments at different sites for studied nanostructured magnetite samples can be determined. The long range ferrimagnetic order provides the dominant contribution to the intensity of the diffraction peak (111) at $d_{hkl} \approx 4.87$ Å, and less pronounced contribution to the peaks (220) at $d_{hkl} \approx 2.98$ Å, (222) at $d_{hkl} \approx 2.43$ Å and (400) at $d_{hkl} \approx 2.08$ Å. The calculated values of ordered iron magnetic moments are listed in Table 2. The RE doping stabilizes the ferrimagnetic ordering in nanostructured magnetites, even slightly increasing the magnetic moment of iron ions in both tetragonal and octahedral oxygen coordination sites. We assumed this is primarily due to a reduction in oxygen defects on the nanoparticle surfaces when RE elements are embeddled in the crystal lattice of magnetite nanoparticles [16, 23, 25].

Magnetic susceptibility measurements

Neutron diffraction data indicate the local ferrimagnetic structure of RE doped magnetite nanoparticles. However, when the nanoparticle size decreases to a critical size [7], the multidomain ferrimagnetism changes to a single-domain state, which is the the essence of the superparamagnetic phenomenon in nanostructured magnetites. To study magnetic properties in more detail, we have studied the magnetic properties of the magnetite nanaparticles through magnetic-field-dependent magnetization $M(H)$ measurements. The magnetization curves of doped magnetite nanoparticles at room temperature with a maximum applied field of 3 T are shown in Fig. 7a. These curves indicate the weak magnetic hysteresis loops for all the nanostructured samples, and the superparamagnetic nature of the studied magnetite nanoparticles is evident. For doped rare earth magnetite, the loop begins to close, suggesting a reduction in coercive force. This can be observed in enlarged section of magnetization curves (Fig. 7b). In case of magnetic measurements on powders, considering the possible interaction between nanoparticles, it is more accurate to analyze the magnetization curves using the Frohlich–Kennelly equation [27]:

$$M(H) = \frac{\chi_i H M_s}{(\chi_i H + M_s)} \tag{4}$$

where χ_i is the initial susceptibility, M_s is saturation magnetization, and H is applied magnetic field. The resulting Frohliche-Kennelly fit for the studied magnetite nanoparticles is shown in Fig. 7c. The values of the initial susceptibility χ_i, coercivity H_c, remanence M_r and saturation M_s magnetization were calculated and are listed in the Table 3.

It can be seen that the magnetization M_s of magnetite nanoparticles doped with rare earth ions decreases by about 20% compared to undoped

Table 3 Calculated magnetic parameters of studied magnetite nanoparticles

Sample	χ_i	M_s (kA/m)	M_r (kA/m)	H_c (kA/m)
Fe_3O_4	15.1(1)	382(3)	48(2)	4.7(2)
La:Fe_3O_4	9.0(2)	314(2)	2(3)	0.3(2)
Lu:Fe_3O_4	12.8(3)	291(2)	16(2)	1.9(3)
Dy:Fe_3O_4	14.9(2)	293(1)	20(1)	2.1(1)
Sm:Fe_3O_4	7.1(2)	305(1)	1(2)	0.2(2)

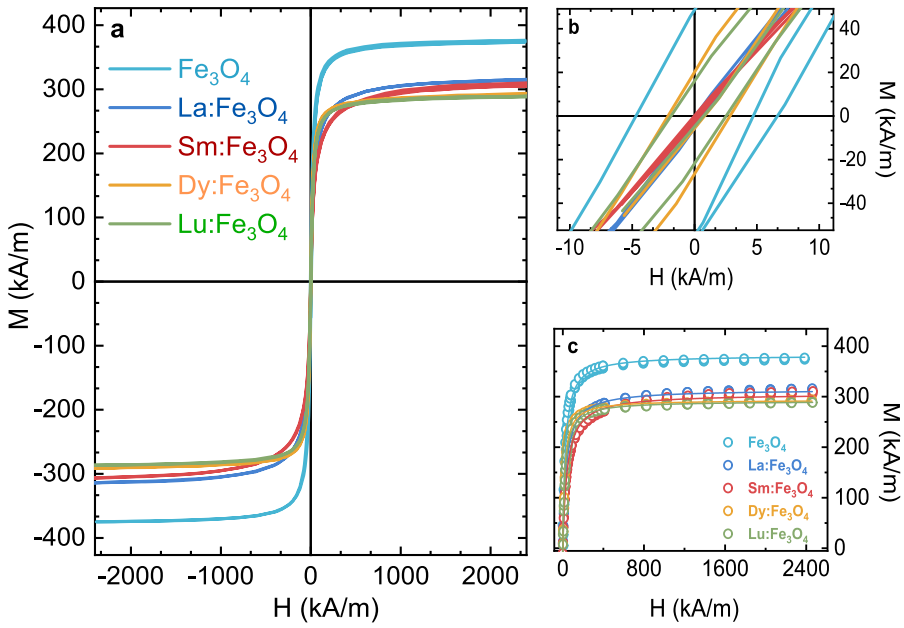

Fig. 7 **a** The magnetization M(H) curves of magnetite nanoparticles doped with rare earth elements RE. **b** The enlarged region of M(H) curves. **c** The Frohlich-Kennelly model fit for nanostructured magnetite compounds. The experimental data are presented in symbols, and the fitting curves obtained using Eq. (4) are shown as solid lines

magnetite. While M_r decreases by about three times for the Lu:Fe_3O_4 and Dy:Fe_3O_4 samples, it decreases by 20-times for the La:Fe_3O_4 sample and by 40-times for the Sm:Fe_3O_4 sample. In the case of nanoparticles, their extremely small size less than 50 nm, and defect-rich surface are the main reasons for this decrease in M_s. This reduction in saturation magnetization can be explained by the lack of oxygen-related superexchange magnetic interaction between surface iron ions. This leads to a decrease in exchange coupling and the tilting of the spin orientation on the surface layer, resulting in the formation of an inactive or "dead" magnetic layer on the nanoparticle surface [1, 23]. As previously reported, the surface-related structural features are the main factor in determining the magnetic properties of ferrite nanoparticles [16, 32]. The coercivity H_c of the doped magnetite nanoparticles is very small, at the level of experimental error, which highlights the superparamagnetic nature of magnetite nanoparticles and their doped samples.

Conclusions

In our work, we prepared a systematic study of the structural and magnetic properties of magnetite nanoparticles doped with rare-earth ions such as Sm, Dy, La, and Lu. These doped nanoparticles were produced by the co-precipitation method, resulting in a series of particles with an average size of not more than 30 nm. The doping process had a dual effect. First, rare-earth ion embedded into the crystal structure of the magnetite caused changes not only in the bond lengths of oxygen units in octahedra but also in the average nanoparticle sizes. As a result, ferromagnetic order state and the average magnetic moments of iron ions of the magnetite phase were partially suppressed. Secondly, doping with rare earth ions is thought to affect disordered structural defects on the nanoparticle surface, reducing interactions between particles and enhancing superparamagnetism phenomena in small magnetite nanoparticles.

Author contributions A.V. Rutkauskas: Funding acquisition, Project administration; O.N. Lis: Investigation (X-ray diffraction), Formal Analysis; S.E. Kichanov: Conceptualization, Formal Analysis, Writing – original draft, Writing—review & editing; B.A. Abdurakhimov: Investigation (X-ray diffraction), Formal Analysis (X-ray diffraction); E.V. Lukin: Investigation (X-ray diffraction, small angle X-ray scattering); D.P. Kozlenko: Funding acquisition, Project administration; A.L. Zhaludkevich: Investigation (sample synthesis); G.S. Rymski and I.I. Makoed: Investigation (Magnetic measurements); A. Mutali: Investigation (TEM).

Funding This work has been supported by the joint grants the Russian Science Foundation, RSF 24–42-10003, https://rscf.ru/project/24-42-10003/ and the Belarusian Foundation for Basic Research, BFBR T23RNFM-023.

Data availability No datasets were generated or analysed during the current study.

Compliance with ethical standards

Conflict of interest The authors declare no competing interests.

References

1. Abdolrahimi M, Vasilakaki M, Slimani S et al (2021) Magnetism of nanoparticles: effect of the organic coating. Nanomaterials 11. https://doi.org/10.3390/nano11071787
2. Alina G, Butler P, Cho J, Doucet M, Kienzle P (2017) Sasview for small angle scattering analysis. https://www.sasview.org/
3. Ansari SAMK, Ficiarà E, Ruffinatti FA et al (2019) Magnetic iron oxide nanoparticles: synthesis, characterization and functionalization for biomedical applications in the central nervous system. Materials (Basel) 12. https://doi.org/10.3390/ma12030465
4. Ba-Abbad MM, Benamour A, Ewis D et al (2022) Synthesis of Fe3O4 nanoparticles with different shapes through a co-precipitation method and their application. JOM 74:3531–3539. https://doi.org/10.1007/s11837-022-05380-3
5. Beaucage G (1996) Small-angle scattering from polymeric mass fractals of arbitrary mass-fractal dimension. J Appl Crystallogr 29:134–146. https://doi.org/10.1107/S0021889895011605
6. Burrows F, Parker C, Evans RFL et al (2010) Energy losses in interacting fine-particle magnetic composites. J Phys D Appl Phys 43:474010. https://doi.org/10.1088/0022-3727/43/47/474010
7. Caizer C (2016) Nanoparticle size effect on some magnetic properties BT - handbook of nanoparticles. In: International S (ed) Aliofkhazraei M. Publishing, Cham, pp 475–519
8. Chen Y-T, Kolhatkar AG, Zenasni O et al (2017) Biosensing using magnetic particle detection techniques. Sensors 17. https://doi.org/10.3390/s17102300
9. de Jesus Andrade Fidelis R, Pires M, de Resende DS et al (2025) Magnetite: properties and applications – a review. J Magn Magn Mater 614:172770. https://doi.org/10.1016/j.jmmm.2025.172770
10. de Jesús Ibarra–Sánchez J, López–Luke T, Ramírez–García G et al (2018) Synthesis and characterization of Fe3O4:Yb3+:Er3+ nanoparticles with magnetic and optical properties for hyperthermia applications. J Magn Magn Mater 465:406–411. https://doi.org/10.1016/j.jmmm.2018.05.091
11. De Teresa JM, Fernández-Pacheco A, Morellon L et al (2007) Magnetotransport properties of Fe3O4 thin films for applications in spin electronics. Microelectron Eng 84:1660–1664. https://doi.org/10.1016/j.mee.2007.01.120
12. Deepak FL, Bañobre-López M, Carbó-Argibay E et al (2015) A systematic study of the structural and magnetic properties of Mn-, Co-, and Ni-doped colloidal magnetite nanoparticles. J Phys Chem C 119:11947–11957. https://doi.org/10.1021/acs.jpcc.5b01575
13. Di Nunzio PE, Stefano M, Bitti RR (2005) Use of Monte Carlo methods in characterizing nanostructured materials by wide- and small-angle X-ray scattering. J Dispers Sci Technol 25:491–501. https://doi.org/10.1081/DIS-200025735
14. Fleet ME (1981) The structure of magnetite. Acta Crystallogr Sect B 37:917–920. https://doi.org/10.1107/S0567740881004597
15. Grüttner C, Müller K, Teller J, Westphal F (2013) Synthesis and functionalisation of magnetic nanoparticles for hyperthermia applications. Int J Hyperth 29:777–789. https://doi.org/10.3109/02656736.2013.835876
16. Gubin SP (2009) Magnetic nanoparticles. John Wiley & Sons, Ltd, Chichester
17. Gürsoy E, Vonbun-Feldbauer GB, Meißner RH (2023) Oxidation-state dynamics and emerging patterns in magnetite. J Phys Chem Lett 14:6800–6807. https://doi.org/10.1021/acs.jpclett.3c01290
18. Hajnorouzi A, Modaresi N (2020) Direct sono electrochemical method for synthesizing Fe3O4 nanoparticles. J Magn Magn Mater 505:166732. https://doi.org/10.1016/j.jmmm.2020.166732
19. Hammouda B (2010) Analysis of the Beaucage model. J Appl Crystallogr 43:1474–1478. https://doi.org/10.1107/S0021889810033856
20. Hu F, Wang D, Ma X et al (2023) Concurrent dual-contrast enhancement using Fe3O4 nanoparticles to achieve a CEST signal controllability. ACS Omega 8:24153–24164. https://doi.org/10.1021/acsomega.2c07000
21. Huan W, Cheng C, Yang Y et al (2012) A study on the magnetic and photoluminescence properties of Eu(n+) and Sm3+ doped Fe3O4 nanoparticles. J Nanosci Nanotechnol 12:4621–4634. https://doi.org/10.1166/jnn.2012.6190
22. Hussein AK (2015) Applications of nanotechnology in renewable energies—a comprehensive overview and understanding. Renew Sustain Energy Rev 42:460–476. https://doi.org/10.1016/j.rser.2014.10.027
23. Issa B, Obaidat IM, Albiss BA, Haik Y (2013) Magnetic nanoparticles: surface effects and properties related to biomedicine applications. Int J Mol Sci 14:21266–21305. https://doi.org/10.3390/ijms141121266
24. Jacobo SE, Duhalde S, Bertorello HR (2004) Rare earth influence on the structural and magnetic properties of NiZn ferrites. J Magn Magn Mater 272–276:2253–2254. https://doi.org/10.1016/j.jmmm.2003.12.564
25. Jain R (2023) Effect of gadolinium doping on the structural, magnetic, electrical, optical, and elastic properties of magnetite nanoparticles. Mater Sci Eng B 296:116631. https://doi.org/10.1016/j.mseb.2023.116631
26. Jain R, Luthra V, Gokhale S (2018) Probing influence of rare earth ions (Er3+, Dy3+ and Gd3+) on structural, magnetic and optical properties of magnetite nanoparticles. J Magn Magn Mater 456:179–185. https://doi.org/10.1016/j.jmmm.2018.02.029
27. Jiles D (2015) Introduction to magnetism and magnetic materials, 3rd edn. CRC Press, Taylor and Francis Group, NY
28. Jing X, Guo M, Li Z et al (2023) Study on structure and magnetic properties of rare earth doped cobalt ferrite: the influence mechanism of different substitution positions. Ceram Int 49:14046–14056. https://doi.org/10.1016/j.ceramint.2022.12.286

29. Ju S, Cai T-Y, Lu H-S, Gong C-D (2012) Pressure-induced crystal structure and spin-state transitions in magnetite (Fe3O4). J Am Chem Soc 134:13780–13786. https://doi.org/10.1021/ja305167h
30. Kalantari S, Shokuhfar A (2024) On the diverse utility of Cu doped ZnS/Fe3O4 nanocomposites. Sci Rep 14:11669. https://doi.org/10.1038/s41598-024-62611-0
31. Kershi RM, Ali FM, Sayed MA (2018) Influence of rare earth ion substitutions on the structural, optical, transport, dielectric, and magnetic properties of superparamagnetic iron oxide nanoparticles. J Adv Ceram 7:218–228. https://doi.org/10.1007/s40145-018-0273-5
32. Koksharov YA (2009) Magnetism of nanoparticles: effects of size, shape, and interactions. In: Gubin SP (ed) Magnetic nanoparticles. John Wiley & Sons, Ltd, Chichester, pp 197–254
33. Kozlenko DP, Dubrovinsky LS, Kichanov SE et al (2019) Magnetic and electronic properties of magnetite across the high pressure anomaly. Sci Rep 9:1–9. https://doi.org/10.1038/s41598-019-41184-3
34. Kozlenko DP, Kichanov SE, Lukin EV, Savenko BN (2021) High-pressure neutron diffraction study of the crystal and magnetic structure of materials at the pulsed reactor IBR-2: current opportunities and prospects. Crystallogr Rep 66:303–313
35. Laha SS, Regmi R, Lawes G (2013) Structural origin for low-temperature relaxation features in magnetic nanoparticles. J Phys D Appl Phys 46:325004. https://doi.org/10.1088/0022-3727/46/32/325004
36. Lak A, Disch S, Bender P (2021) Embracing defects and disorder in magnetic nanoparticles. Adv Sci 8:2002682. https://doi.org/10.1002/advs.202002682
37. Langford JI, Wilson AJC (1978) Scherrer after sixty years: a survey and some new results in the determination of crystallite size. J Appl Crystallogr 11:102–113. https://doi.org/10.1107/S0021889878012844
38. Lastovina TA, Bugaev AL, Kubrin SP et al (2016) Structural studies of magnetic nanoparticles doped with rare-earth elements. J Struct Chem 57:1444–1449. https://doi.org/10.1134/S0022476616070209
39. Levish A, Joshi S, Winterer M (2023) Chemical vapor synthesis of nanocrystalline iron oxides. Appl Energy Combust Sci 15:100177. https://doi.org/10.1016/j.jaecs.2023.100177
40. Li H, Kobayashi M, Kou S et al Noncollinear magnetism in Fe3O4 induced via site-selective rare-earth substitution boosting its saturation magnetization. Small n/a:2411133. https://doi.org/10.1002/smll.202411133
41. Li Q, Kartikowati CW, Horie S et al (2017) Correlation between particle size/domain structure and magnetic properties of highly crystalline Fe3O4 nanoparticles. Sci Rep 7:9894. https://doi.org/10.1038/s41598-017-09897-5
42. Li T, Senesi AJ, Lee B (2016) Small angle X-ray scattering for nanoparticle research. Chem Rev 116:11128–11180. https://doi.org/10.1021/acs.chemrev.5b00690
43. Licciardi M, Scialabba C, Fiorica C et al (2013) Polymeric nanocarriers for magnetic targeted drug delivery: preparation, characterization, and in vitro and in vivo evaluation. Mol Pharm 10:4397–4407. https://doi.org/10.1021/mp300718b
44. Monalisa SS, Satyapal HK, Singh RK (2021) Correlation between lattice strain and magnetic properties enhancement of nanocrystalline cobalt ferrite with controlled annealing. J Mater Sci Mater Electron 32:23843–23853. https://doi.org/10.1007/s10854-021-06795-5
45. Monshi A, Foroughi MR, Monshi MR (2012) Modified Scherrer equation to estimate more accurately nano-crystallite size using XRD. World J Nano Sci Eng 02:154–160. https://doi.org/10.4236/wjnse.2012.23020
46. Nedelkoski Z, Kepaptsoglou D, Lari L et al (2017) Origin of reduced magnetization and domain formation in small magnetite nanoparticles. Sci Rep 7:45997. https://doi.org/10.1038/srep45997
47. O'Neill HSC, Navrotsky A (1983) Simple spinels: crystallographic parameters, cation radii, lattice energies, and cation distribution. Am Mineral 68:181–194
48. Padalia D, Johri UC, Zaidi MGH (2012) Study of cerium doped magnetite (Fe3O4:Ce)/PMMA nanocomposites. Phys B Condens Matter 407:838–843. https://doi.org/10.1016/j.physb.2011.12.016
49. Paula FL de O (2019) SAXS analysis of magnetic field influence on magnetic nanoparticle clusters. Condens Matter 4:. https://doi.org/10.3390/condmat4020055
50. Pauw BR, Pedersen JS, Tardif S et al (2013) Improvements and considerations for size distribution retrieval from small-angle scattering data by Monte Carlo methods. J Appl Crystallogr 46:365–371. https://doi.org/10.1107/S0021889813001295
51. Peng J, Hojamberdiev M, Xu Y et al (2011) Hydrothermal synthesis and magnetic properties of gadolinium-doped CoFe2O4 nanoparticles. J Magn Magn Mater 323:133–137. https://doi.org/10.1016/j.jmmm.2010.08.048
52. Polozhentsev OE, Kubrin SP, Butova VV et al (2016) Structure and magnetic properties of pure and samarium doped magnetite nanoparticles. J Struct Chem 57:1459–1468. https://doi.org/10.1134/S0022476616070222
53. Rego GN de A, Mamani JB, Souza TKF et al (2019) Therapeutic evaluation of magnetic hyperthermia using Fe3O4-aminosilane-coated iron oxide nanoparticles in glioblastoma animal model. Einstein (Sao Paulo) 17:eAO4786. https://doi.org/10.31744/einstein_journal/2019AO4786
54. Rodríguez-Carvajal J (1993) Recent advances in magnetic structure determination by neutron powder diffraction. Phys B Condens Matter 192:55–69. https://doi.org/10.1016/0921-4526(93)90108-I
55. Rosická D, Šembera J (2011) Influence of structure of iron nanoparticles in aggregates on their magnetic properties. Nanoscale Res Lett 6:527. https://doi.org/10.1186/1556-276X-6-527
56. Schneider CA, Rasband WS, Eliceiri KW (2012) NIH Image to ImageJ: 25 years of image analysis. Nat Methods 9:671–675. https://doi.org/10.1038/nmeth.2089
57. Semaltianos NG, Karczewski G (2021) Laser synthesis of magnetic nanoparticles in liquids and application in the fabrication of polymer–nanoparticle composites. ACS Appl Nano Mater 4:6407–6440. https://doi.org/10.1021/acsanm.1c00715
58. Sonia LC, Kuldeep, Basheed GA, Phanjoubam S (2024) Influence of rare earth (RE = Y, La, Gd, Ho) substitution on the structural, magnetic and rheological properties

of magnetite based ferrofluids. J Magn Magn Mater 592:171779. https://doi.org/10.1016/j.jmmm.2024.171779
59. Srinoi P, Chen Y-T, Vittur V et al (2018) Bimetallic nanoparticles: enhanced magnetic and optical properties for emerging biological applications. Appl Sci 8. https://doi.org/10.3390/app8071106
60. Srivastava V, Singh P, Weng C, Sharma Y (2011) Economically viable synthesis of Fe3O4 nanoparticles and their characterization. Polish J Chem Technol 13:1–5. https://doi.org/10.2478/v10026-011-0015-8
61. Stevanović V, D'Avezac M, Zunger A (2010) Simple point-ion electrostatic model explains the cation distribution in spinel oxides. Phys Rev Lett 105:11–14. https://doi.org/10.1103/PhysRevLett.105.075501
62. Svergun DI (1992) Determination of the regularization parameter in indirect-transform methods using perceptual criteria. J Appl Crystallogr 25:495–503. https://doi.org/10.1107/S0021889892001663
63. Svergun DI (2010) Small-angle X-ray and neutron scattering as a tool for structural systems biology. 391:737–743. https://doi.org/10.1515/bc.2010.093
64. Tatarchuk T (2024) Studying the defects in spinel compounds: discovery, formation mechanisms, classification, and influence on catalytic properties. Nanomaterials 14. https://doi.org/10.3390/nano14201640
65. Upadhyay S, Parekh K, Pandey B (2016) Influence of crystallite size on the magnetic properties of Fe3O4 nanoparticles. J Alloys Compd 678:478–485. https://doi.org/10.1016/j.jallcom.2016.03.279
66. Wang Y, Liu X, Ma S et al (2023) Progress in cancer therapy with functionalized Fe3O4 nanomaterials. Front Mater Sci 17:230658. https://doi.org/10.1007/s11706-023-0658-4
67. Wei Y, Han B, Hu X et al (2012) Synthesis of Fe3O4 nanoparticles and their magnetic properties. Procedia Eng 27:632–637. https://doi.org/10.1016/j.proeng.2011.12.498
68. Yang Y, Huang M, Qian J et al (2020) Tunable Fe3O4 nanorods for enhanced magnetic hyperthermia performance. Sci Rep 10:8331. https://doi.org/10.1038/s41598-020-65095-w
69. Zeng M, Thummavichai K, Chen W et al (2021) Study on the mechanism of tunable ferromagnetic composites with different rare earth ions. RSC Adv 11:37246–37253. https://doi.org/10.1039/D1RA07249H